Nocturnal Relative Humidity Maxima above the Boundary Layer in the U.S. Midwest: A Diagnostic for the Mountain–Plains Solenoidal Circulation

AMANDA MERCER, RACHEL CHANG, AND IAN FOLKINS

Department of Physics and Atmospheric Science, Dalhousie University, Halifax, Nova Scotia, Canada

(Manuscript received 29 June 2017, in final form 12 January 2018)

ABSTRACT

Measurements from the Aircraft Communications, Addressing, and Reporting System (ACARS) dataset between 2005 and 2014 are used to construct diurnal vertical cross sections of relative humidity in the lower troposphere at six airports in the U.S. Midwest. In summer, relative humidity maxima occur between 2 and 3 km during the overnight hours of 0300–0900 local solar time (LST). These maxima coincide with negative anomalies in temperature and positive anomalies in specific humidity. Vertical winds from the Modern-Era Retrospective Analysis for Research and Applications, version 2 (MERRA-2), reanalysis dataset show that the height and diurnal timing of these positive relative humidity anomalies are consistent with the regional diurnal pattern of vertical motion. During the day, there is rising motion over the Rocky Mountains and subsidence over the Midwest, while conversely at night, there is sinking motion over the mountains and rising motion over the Midwest. The nocturnal relative humidity maxima over the Midwest are the strongest direct observational evidence to date of this mountain–plains solenoidal circulation, and provide a useful diagnostic for testing the strength of this circulation in climate and reanalysis models. There is significant interannual variability in the strength of the nocturnal relative humidity maxima. In 2011, the relative humidity maxima are very pronounced. In 2014, however, they are almost nonexistent. Finally, the relative humidity maxima are discussed in relation to the low-level jet (LLJ). The LLJ appears to be too low to directly contribute to the nocturnal relative humidity maxima.

1. Introduction

Boundary layer turbulence is mainly generated by low-level wind shear and convective instability, and usually gives rise to an upward eddy moisture flux from the surface. Because of the requirement that potential temperature increase with height in a stable atmosphere, strong boundary layer turbulence also tends to cool the upper part of a well-mixed boundary layer. The combination of these turbulent moisture and heat fluxes tends to decrease relative humidity near the surface, and increase relative humidity in the upper part of the boundary layer. Observations of the diurnal and vertical variation of relative humidity within the boundary layer are, therefore, an important diagnostic of the strength of boundary layer turbulence, and of the propensity of a boundary layer to support cloud development.

The diurnal variation of relative humidity in the lower troposphere can also be used to diagnose the existence of diurnal changes in large-scale vertical motion. These motions can be generated by tidal circulations, sea-breeze circulations, or circulations generated by orographic heating. Several modeling studies have indicated the presence of a large-scale diurnal variation in vertical motion, often called the mountain–plains solenoid, which is associated with diurnal variations in heating over mountain regions. The term "solenoid" refers to the vertical circulations that develop in response to baroclinic environments over sloping terrain. This circulation has been studied over the eastern slopes of mountain ranges, such as the U.S. Rocky Mountains (Tripoli and Cotton 1989; Wolyn and McKee 1994; Bossert et al. 1989), the Tibetan Plateau (Sun and Zhang 2012), the Yanshan–Taihangshan Mountains (Bao and Zhang 2013), and the Andes (Nicolini and Skabar 2011; Repinaldo et al. 2015).

Reanalysis datasets have been used to study the vertical motion field over the eastern slopes of the Rocky Mountains (Tuttle and Davis 2013; Carbone and Tuttle 2008; Trier et al. 2010). During the day, there is upward motion over the mountains and downward motion over the adjacent plains. Overnight, there is a reversal in the vertical motion field with subsidence over the mountains and

Corresponding author: Amanda Mercer, amanda.mercer@dal.ca

DOI: 10.1175/MWR-D-17-0189.1

upward motion over the plains. It has also been shown that the mountain–plains solenoidal circulation contributes to ozone exceedances along the Colorado Front Range, and that it exports boundary layer pollutants into the free troposphere (Sullivan et al. 2016). Similarly, recent work has been done in the eastern United States regarding boundary layer winds and air pollution events (Rabenhorst et al. 2014). The strength of the solenoidal circulation is believed to be sensitive to surface properties such as soil moisture, the strength of the ambient winds (westerlies), and solar heating (Wolyn and McKee 1994). Interactions between the solenoidal circulation and other heat sources such as deep convection are not well understood.

Figure 1 shows a diagram of the principal heat sources and circulations between the U.S. Rocky Mountains and the adjacent plains during the overnight hours. At night, there is longwave radiative cooling over the mountains. Differential cooling of the air over the eastern slopes creates a horizontal temperature gradient and a subsequent westerly downslope flow in the lower troposphere, with rising motion over the plains. The solenoidal circulation is indicated by the green arrows. Second, over the U.S. plains, there is a diurnal cycle in convective rainfall with a peak at night (Carbone and Tuttle 2008; Li and Smith 2010; Tuttle and Davis 2013; Zhang et al. 2014). It has been suggested that this nocturnal peak in rainfall is related to the nocturnal upward motion associated with the mountain–plains solenoid (Carbone and Tuttle 2008; Tuttle and Davis 2013; Trier et al. 2010). Convective heating itself would also be expected to modify the vertical motion field. Finally, differential solar heating of the lower troposphere between the continents and oceans creates a thermal low over the interior of North America during summer, with prevailing southwesterly large-scale flow near the surface at 95°W. Observations of lower-tropospheric relative humidity over the full diurnal cycle can be used as a diagnostic for the net residual vertical circulation generated by the diurnal variation of these various heat sources.

We use commercial aircraft measurements from the Aircraft Communications, Addressing, and Reporting System (ACARS; Moninger et al. 2003) to characterize the diurnal and vertical variation of lower-tropospheric relative humidity at six midwestern and two mountain airports. These data are continuously available from July 2001 to the present, and have reasonably good coverage throughout the boundary layer. We focus on overnight relative humidity maxima that are observed near 2.5 km during the summer. Section 2 describes the ACARS and other datasets used. Section 3 shows diurnal vertical cross sections of relative humidity at the eight sites during the summer using data from 2005 to 2014. We also show diurnal cross sections of temperature and specific humidity at Dallas, Texas, and Kansas City, Missouri. Section 4 discusses the interannual variability of the lower-tropospheric relative humidity anomalies. In section 5, we show the spatial and diurnal variation of 750-hPa vertical motion, as well as mean vertical cross sections of vertical motion, from Modern-Era Retrospective Analysis for Research and Applications, version 2 (MERRA-2), reanalysis data. Finally, the nocturnal low-level jet (LLJ) is an important source of moisture to the Midwest (Berg et al. 2015; Pitchford and London 1962; Higgins et al. 1997; Whiteman et al. 1997). Section 6 discusses the direction and height of the LLJ in relation to overnight relative humidity anomalies. At most midwestern locations, the LLJ is below 2 km. It is, therefore, not expected to directly contribute to the 2.5-km nocturnal relative humidity maxima.

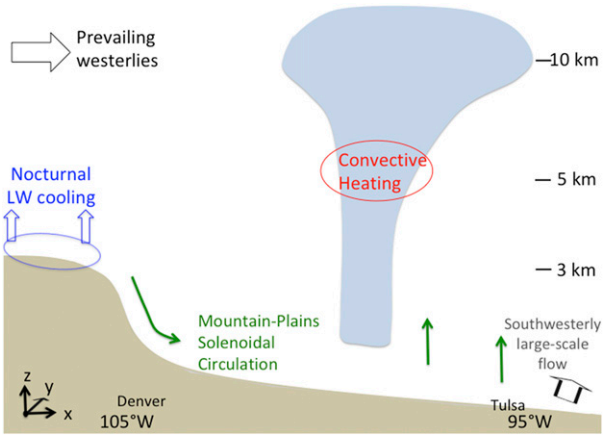

FIG. 1. Diagram showing the principal heat sources and sinks over the U.S. Midwest at night. The green arrows illustrate the mountain–plains solenoidal circulation, with downslope flow over the mountains and rising motion over the plains. Nocturnal rainfall over the plains at night gives rise to convective heating of the lower troposphere that is largest in the midtroposphere. The locations of Denver and Tulsa are shown for geographic reference.

2. Datasets

a. Meteorological data from commercial aircraft

The ACARS dataset is stored within the Meteorological Assimilation Data Ingest System (MADIS), run by the National Oceanic and Atmospheric Administration (NOAA). The dataset includes measurements of aircraft location, altitude, time of day, temperature, dewpoint temperature, relative humidity, wind speed, and wind direction. Data are available from July 2001 to the present.

We focus on data collected during landings and takeoffs at eight airports during 2005–14. These airports are as follows: (i) Phoenix, Arizona; (ii) Denver, Colorado; (iii) Houston, Texas; (iv) Dallas, Texas; (v) Tulsa, Oklahoma; (vi) Kansas City, Missouri; (vii) St. Louis, Missouri; and (viii) Chicago, Illinois. These sites were

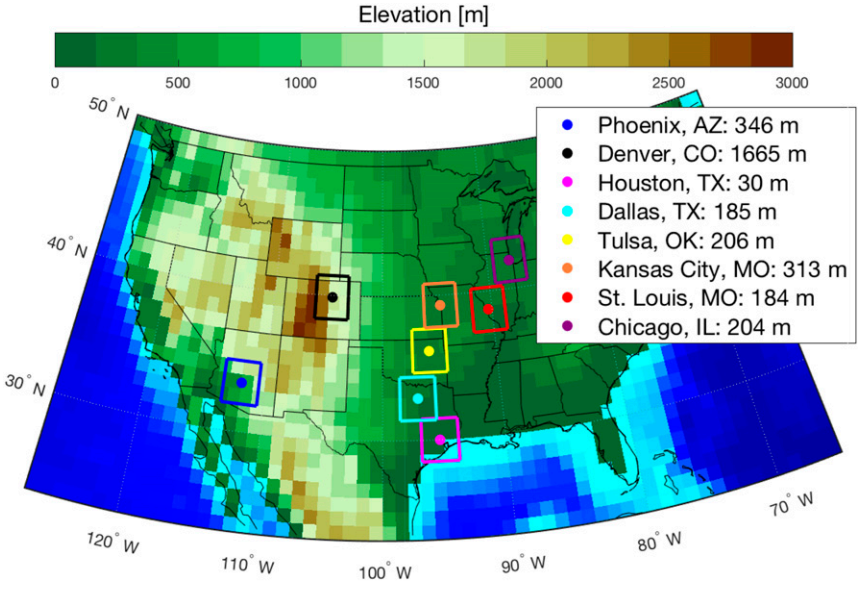

FIG. 2. Map of midwestern airports and defined 3° latitude by 3° longitude boxes surrounding them. The background colors represent topography, where brown corresponds to higher elevations above sea level. The elevation of each airport is also listed in the legend.

chosen because they have a larger volume of data and greater diurnal coverage than other midwestern and mountain locations. We define 3° latitude by 3° longitude boxes surrounding each airport. These boxes, as well as the airport locations (dots) are shown in Fig. 2. Aircraft data within each box are assigned to 200-m altitude and hourly local solar time (LST) bins. Outliers within each airport box and time–height bin are detected and screened out according to the interquartile range rule. The interquartile range represents the spread of the middle 50% of data. It is defined as the difference between the upper and lower quartiles of data. Measurements that fall more than 1.5 times the interquartile range lower in magnitude than the lower quartile or higher in magnitude than the upper quartile are detected and screened out. After this screening process, the remaining data in each box and time–height bin are averaged over each month of each year. LST is calculated from observed time of day (UTC) and longitude.

To visualize the diurnal coverage in ACARS data, Fig. 3 shows a contour plot indicating the number of June–August (JJA) relative humidity measurements available in Dallas over the years 2005–14 within each LST–altitude bin. Between 0500 and 2200 LST, there are usually between 500 and 2000 measurements per hour within a 200-m height bin. During the overnight hours from 2200 to 0430 LST, the coverage is much less, with typically fewer than 200 measurements per hour within a 200-m height bin.

There have been efforts by various government agencies to implement quality control on the ACARS data for use in numerical weather prediction models (Moninger et al. 2003). The accuracy of ACARS temperature and wind data over the western and central United States has also been tested through collocation statistics (Benjamin et al. 1999). They determined the error in boundary layer temperature and winds to be 0.72 K and 2.5 m s^{-1}, respectively. ACARS temperature and wind measurements at Denver have also been tested through rawinsonde comparison (Schwartz and Benjamin 1995). They determined average differences of 0.59 K and 4 m s^{-1}

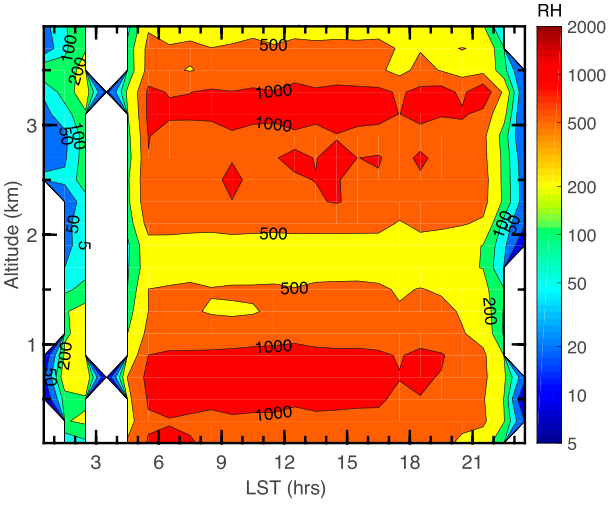

FIG. 3. Number of ACARS relative humidity measurements per LST–height bin, available in the Dallas area during JJA 2005–14.

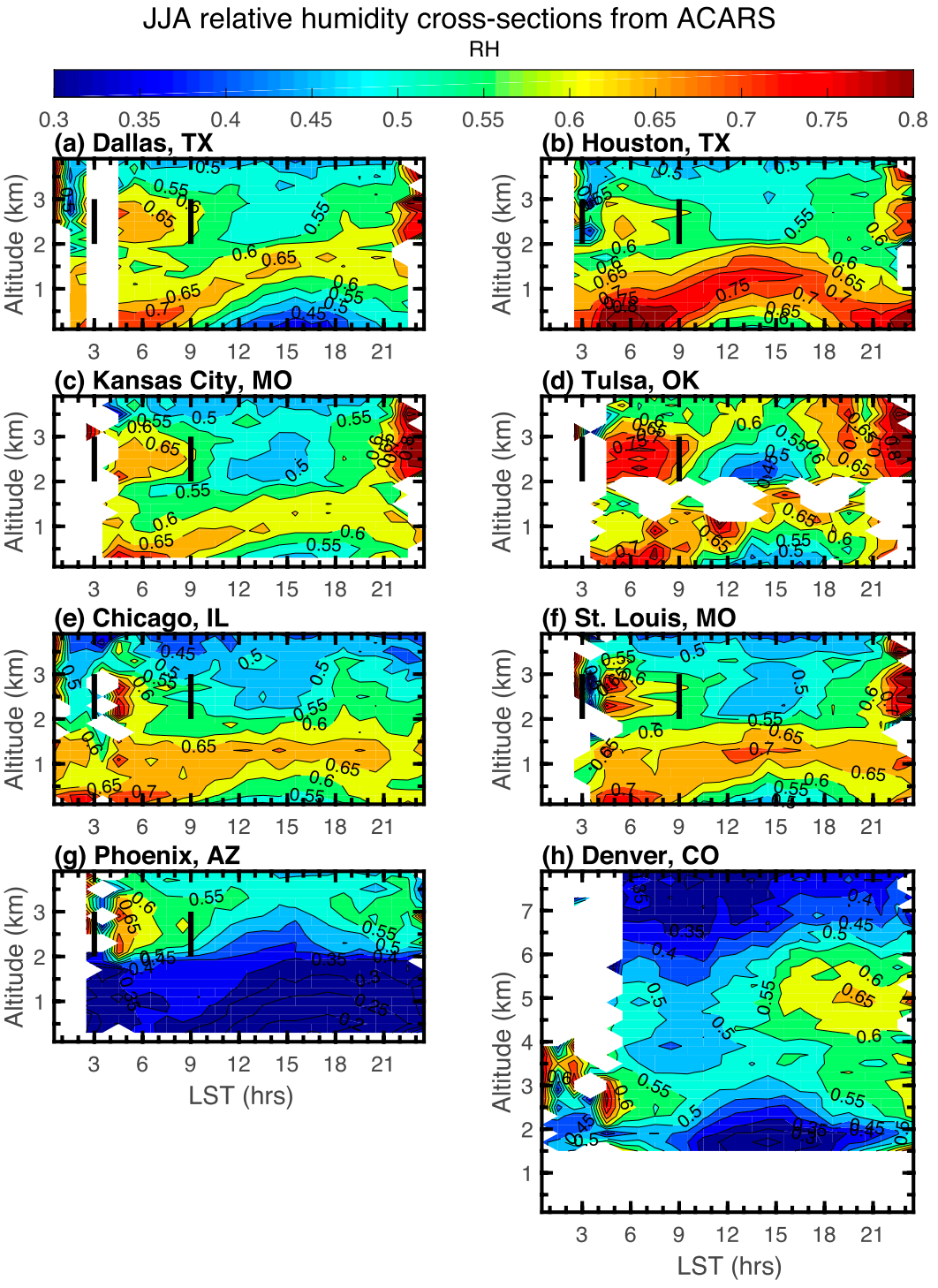

FIG. 4. ACARS JJA cross sections of relative humidity at (a) Dallas, (b) Houston, (c) Kansas City, (d) Tulsa, (e) Chicago, (f) St. Louis, (g) Phoenix, and (h) Denver. Data from JJA of 2005–14 are used. Note the nocturnal local maxima in relative humidity between 2 and 3 km from roughly 0300 to 0900 LST at the six midwestern airports and Phoenix, as indicated by the black vertical lines.

for temperature and wind, respectively, within a 25-km distance. Additionally, dewpoint temperature data from ACARS have been compared to radiosonde data over the continental United States (Mamrosh et al. 2002). They estimated an average dewpoint difference of 1.9 K within a 50-km distance.

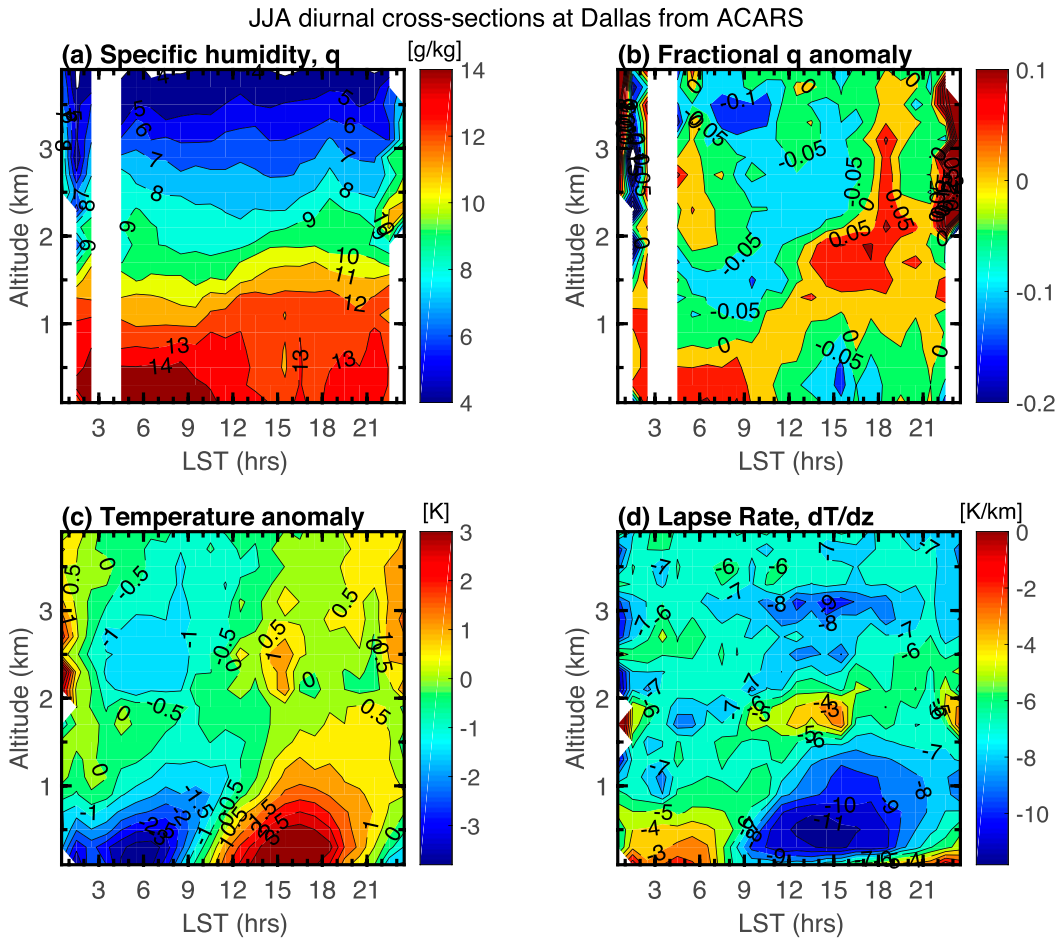

FIG. 5. ACARS JJA cross sections of (a) specific humidity q ($g\,kg^{-1}$), (b) fractional q anomaly, (c) temperature anomaly (K), and (d) lapse rate ($K\,km^{-1}$) at Dallas.

b. Vertical motion from MERRA-2 reanalysis

The MERRA-2 reanalysis data (Gelaro et al. 2017) are managed by the NASA Goddard Earth Sciences (GES) Data and Information Services Center (DISC). The assimilated meteorological data are on a 0.5° latitude by 0.625° longitude grid, with a 3-h temporal resolution and 42 vertical levels. MERRA-2 assimilates in situ and satellite observations (McCarty et al. 2016).

We used the three-dimensional assimilated meteorological fields (GMAO 2015) dataset, which includes vertical motion and relative humidity data. To be consistent with the ACARS time period, we focus on JJA data from 2005 to 2014.

3. Relative humidity maxima above the boundary layer

We used the ACARS measurements to construct cross sections of the mean diurnal variation of lower-tropospheric relative humidity at each of the eight airport locations shown in Fig. 2. These diurnal vertical cross sections are shown in Fig. 4. Each cross section was constructed from measurements during JJA from 2005 to 2014. For each month, measurements are averaged within time–height bins if there are at least 10 measurements in a given bin. Each monthly climatology is given an equal contribution to the overall summer climatology over the 10 years. White spaces indicate that there are no data within a time–height bin or that the data have been screened out.

Cross sections from the six midwestern airport locations (i.e., excluding Phoenix and Denver) are broadly similar. They show a relative humidity minimum near the surface during the day and higher relative humidity near the surface at night. During the day, there is a maximum in relative humidity at the top of the convective boundary layer that reaches a peak near 1500 LST between 1.5 and 2 km. In addition, 7 of the 8 locations show a local maximum in relative humidity between 2 and 3 km above the surface during the early morning hours (roughly 0300–0900 LST).

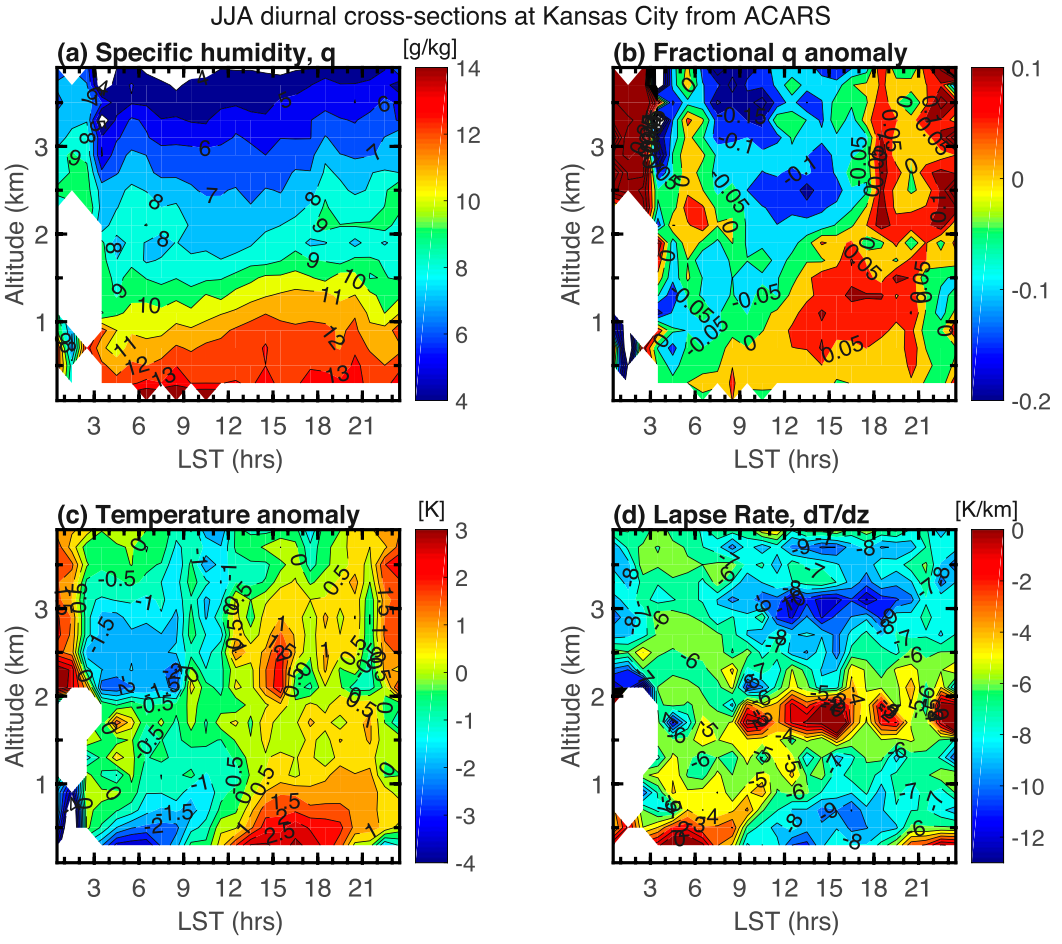

FIG. 6. ACARS JJA cross sections of (a) specific humidity q (g kg^{-1}), (b) fractional q anomaly, (c) temperature anomaly (K), and (d) lapse rate (K km^{-1}) at Kansas City.

At Denver, a relative humidity maximum 2–4 km above the surface (i.e., roughly 4–6 km above sea level) appears in the late afternoon and persists after sunset.

Positive anomalies in relative humidity can arise from positive anomalies in specific humidity q or negative anomalies in temperature. Figures 5a and 5b show JJA mean diurnal cross sections of q and the fractional anomaly in q at Dallas. Specific humidity was derived from aircraft measurements of dewpoint temperature and pressure–altitude. At a given height, the fractional anomaly in q was defined as the deviation from the 24-h average normalized by the 24-h average. Figure 5a shows that the q contours tilt upward in the morning and early afternoon, and generate a strong positive q anomaly between 1 and 2 km during the day. This is presumably the result of upward turbulent and convective transport of moisture during the day. There is also a positive q anomaly overnight between 2 and 2.5 km.

Figure 5c shows the JJA lower-tropospheric diurnal temperature anomalies at Dallas. There is a positive temperature anomaly starting at the surface in late morning. The vertical tilt of the anomaly presumably reflects the upward transport of sensible heat from the surface. After sunset, there is a negative temperature anomaly near the surface. The negative temperature anomaly between 2 and 3 km from 0300 to 0900 LST is coincident with the overnight relative humidity maximum at Dallas. The overnight positive relative humidity anomaly between 2 and 3 km at Dallas is, therefore, associated with both a negative anomaly in temperature and a positive anomaly in specific humidity. These anomalies are consistent with nocturnal upward motion in the lower troposphere (e.g., from the mountain–plains solenoid).

Figure 5d shows Dallas JJA mean diurnal cross sections of lapse rate (here dT/dz). Lapse rates are calculated from the mean temperature cross sections. Overnight, the stable boundary layer (SBL) is indicated by the more stable lapse rates near the surface. By afternoon, there is a stable layer (‘‘inversion’’) at a height of 2 km. This is coincident with the height of the daytime

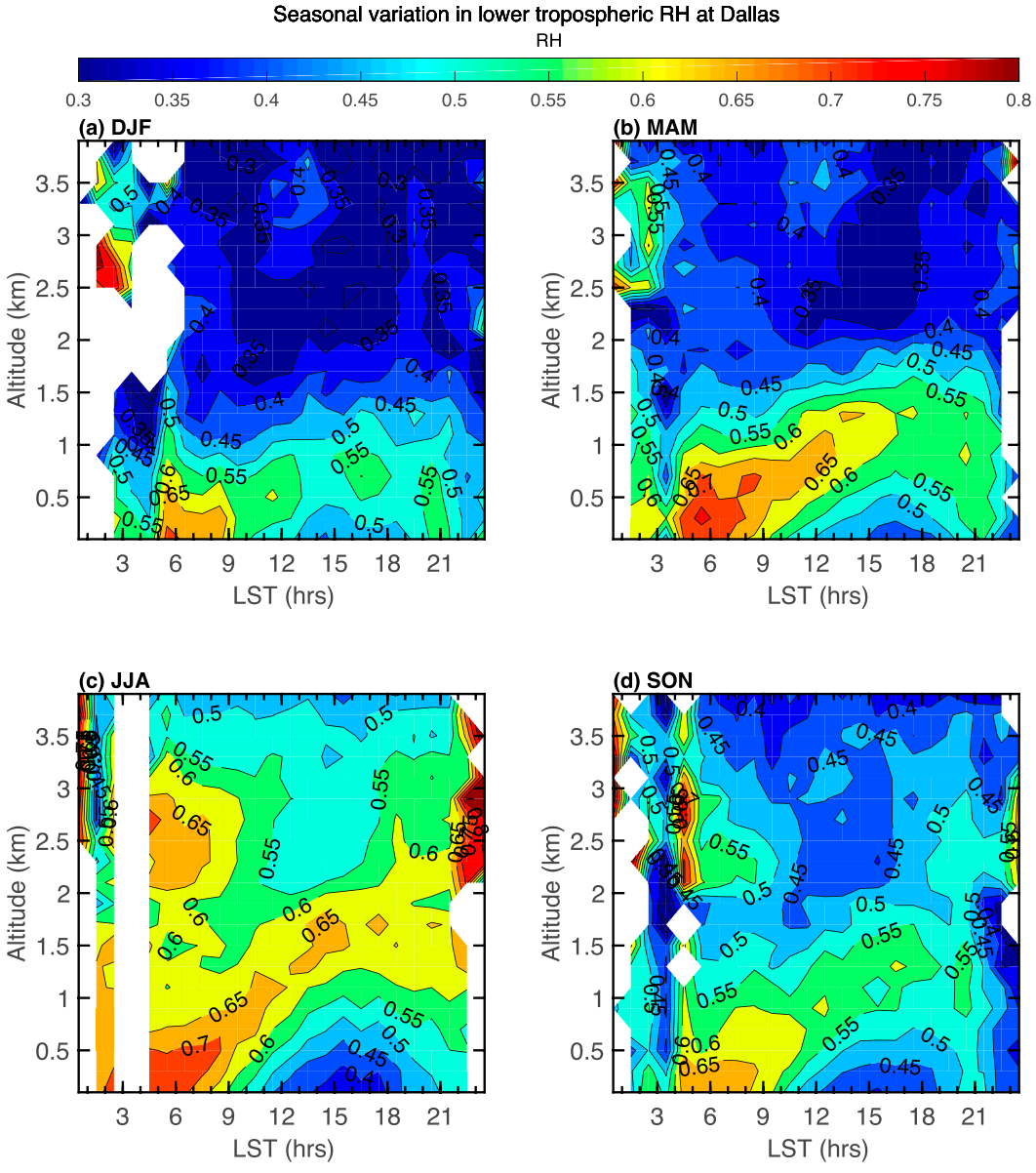

FIG. 7. ACARS cross sections of relative humidity during (a) DJF, (b) MAM, (c) JJA, and (d) SON at Dallas. The nocturnal relative humidity maxima are strongest during the summer but persist to some degree into the fall.

relative humidity maximum from Fig. 4a. Below the daytime capping stable layer, unstable lapse rates occur in the convective boundary layer.

Figure 6 shows diurnal climatological cross sections of q, q anomaly, temperature anomaly, and lapse rate at Kansas City. The overall patterns are quite similar to Dallas. Again, there is both a positive q anomaly and a negative temperature anomaly overnight between 2 and 3 km, so that the nocturnal relative humidity maximum can again be attributed to both a decrease in temperature and an increase in q. In Fig. 6c, the diurnal variation in temperature between 2 and 3 km is almost as strong as the diurnal temperature variation near the ground. In Fig. 6d, the inversion at the top of the daytime boundary layer is stronger at Kansas City than at Dallas and forms earlier in the morning.

Figure 7 shows the seasonal variation of lower-tropospheric relative humidity at Dallas. The daytime relative humidity maximum near the top of the boundary layer is strongest during the summer (JJA) and weakest during the winter [December–February (DJF)]. It is also highest in altitude during the summer and lowest in altitude during the winter. The 2–3-km overnight relative humidity maximum is strongest during the summer, but is present to some degree

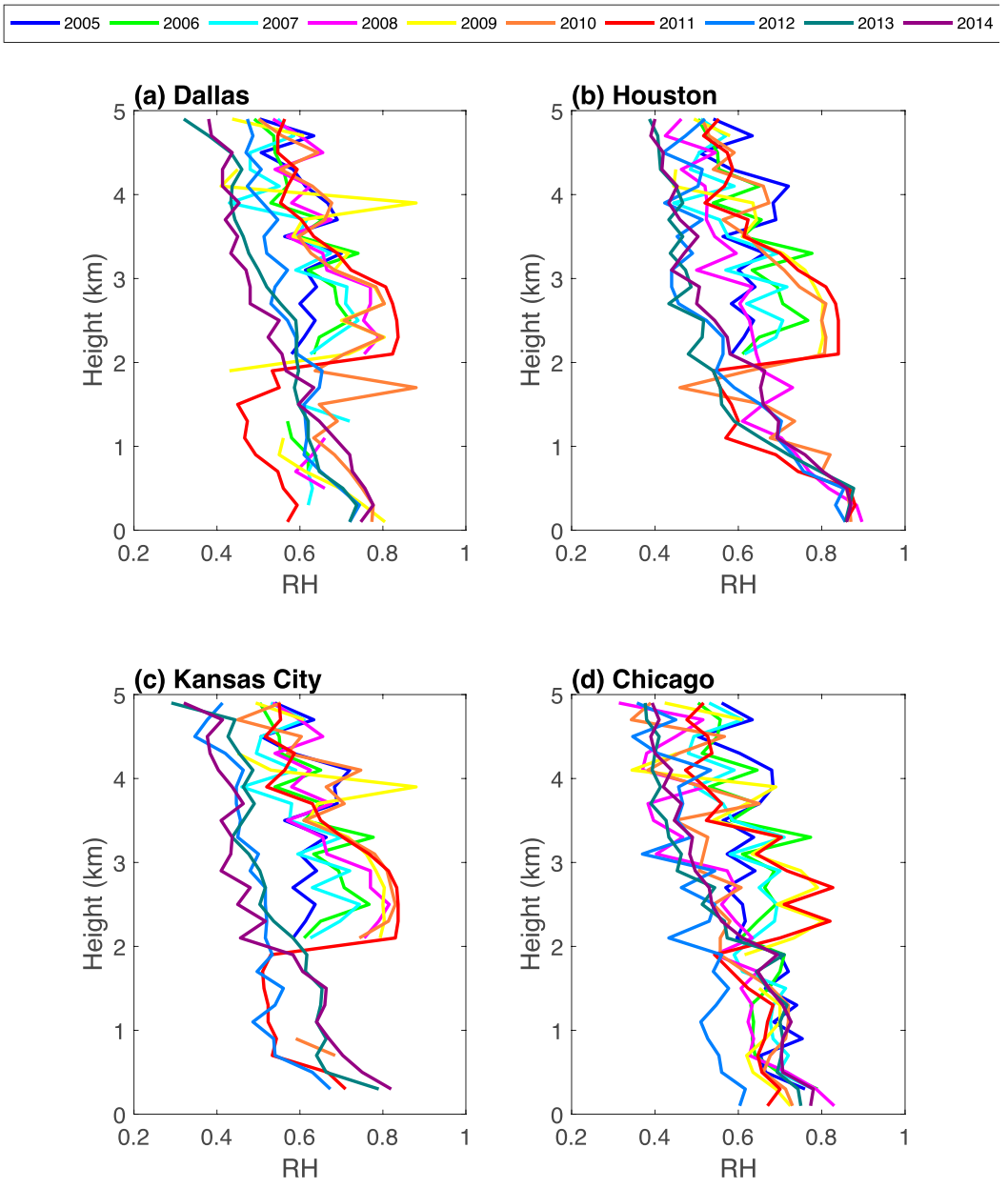

FIG. 8. Interannual variation in JJA vertical profiles of relative humidity near 0500 LST at (a) Dallas, (b) Houston, (c) Kansas City, and (d) Chicago over the 10-yr period, 2005–14. The overnight 2.5-km relative humidity maxima are strongest in 2009, 2010, and 2011.

in the fall [September–November (SON)]. The seasonal variation of the strength of the nocturnal relative humidity maximum therefore appears to be roughly in phase with solar heating.

4. Interannual variability in lower-tropospheric relative humidity

The nocturnal relative humidity maxima have significant interannual variability. Figure 8 shows the JJA mean relative humidity profiles at 0500 LST of four midwestern airports for individual years between 2005 and 2014. Each year in the 10-yr period is represented by a different color. At Dallas, Houston, and Kansas City, the 2–3-km nocturnal relative humidity maximum is strongest in 2011 (red), 2010 (orange), and 2009 (yellow). In the remaining years, it is only weakly present, if at all.

Figure 9 shows JJA diurnal vertical cross sections of relative humidity at each airport location during 2011. This is the year with the strongest 2–3-km nocturnal relative

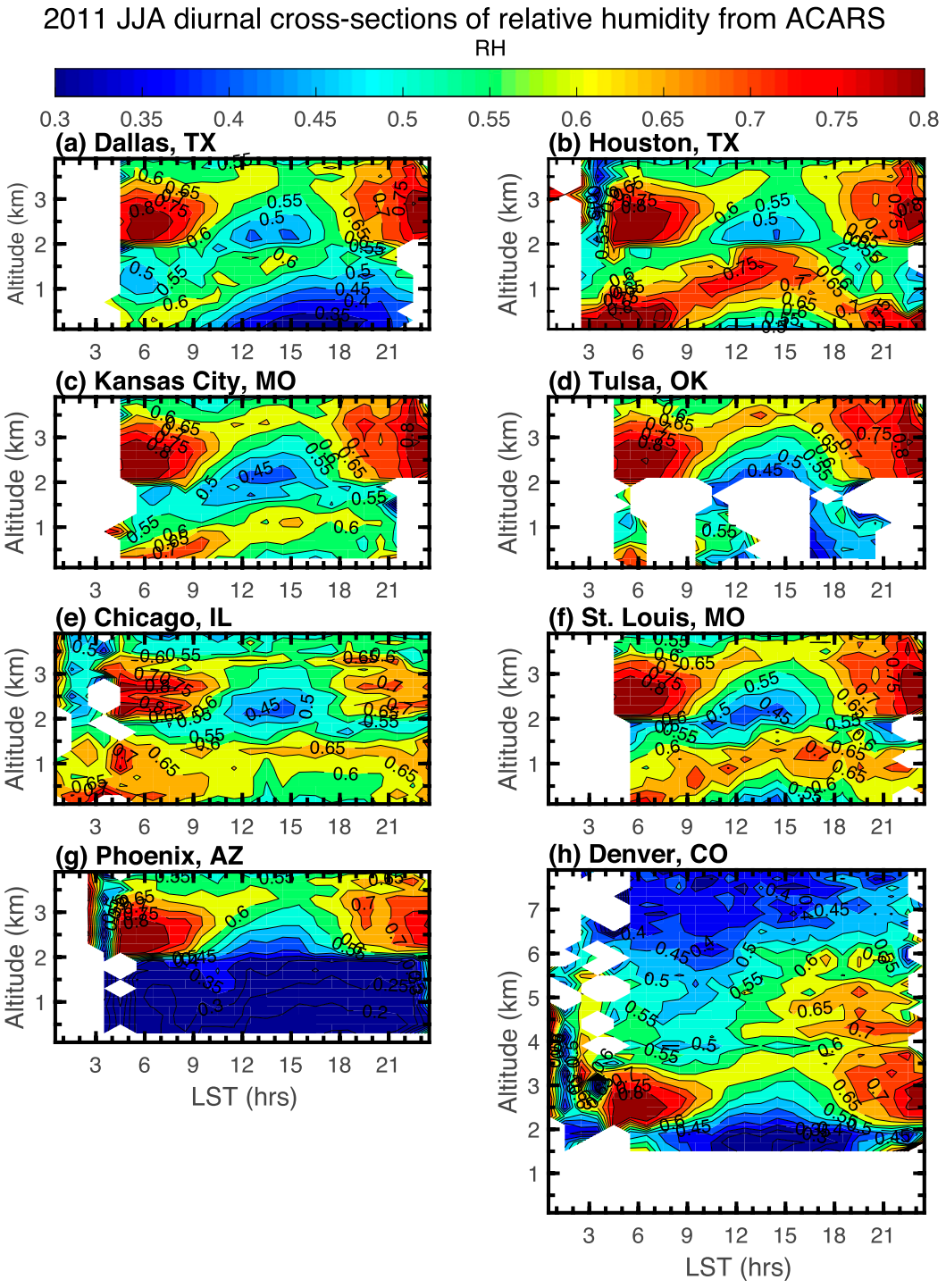

FIG. 9. JJA 2011 cross sections of relative humidity at (a) Dallas, (b) Houston, (c) Kansas City, (d) Tulsa, (e) Chicago, (f) St. Louis, (g) Phoenix, and (h) Denver. Strong nocturnal relative humidity maxima occur near 2.5 km at all six midwestern locations and Phoenix.

humidity maxima. They are present at all seven locations other than Denver, and appear to start at 1800 LST. At Denver, there is again a late afternoon maximum between 4 and 6 km. During the spring and summer of 2011, there was a severe drought in Texas, Oklahoma, and southern Kansas (Smith et al. 2017). The relevance of this drought to the observed nocturnal relative humidity maxima is unclear.

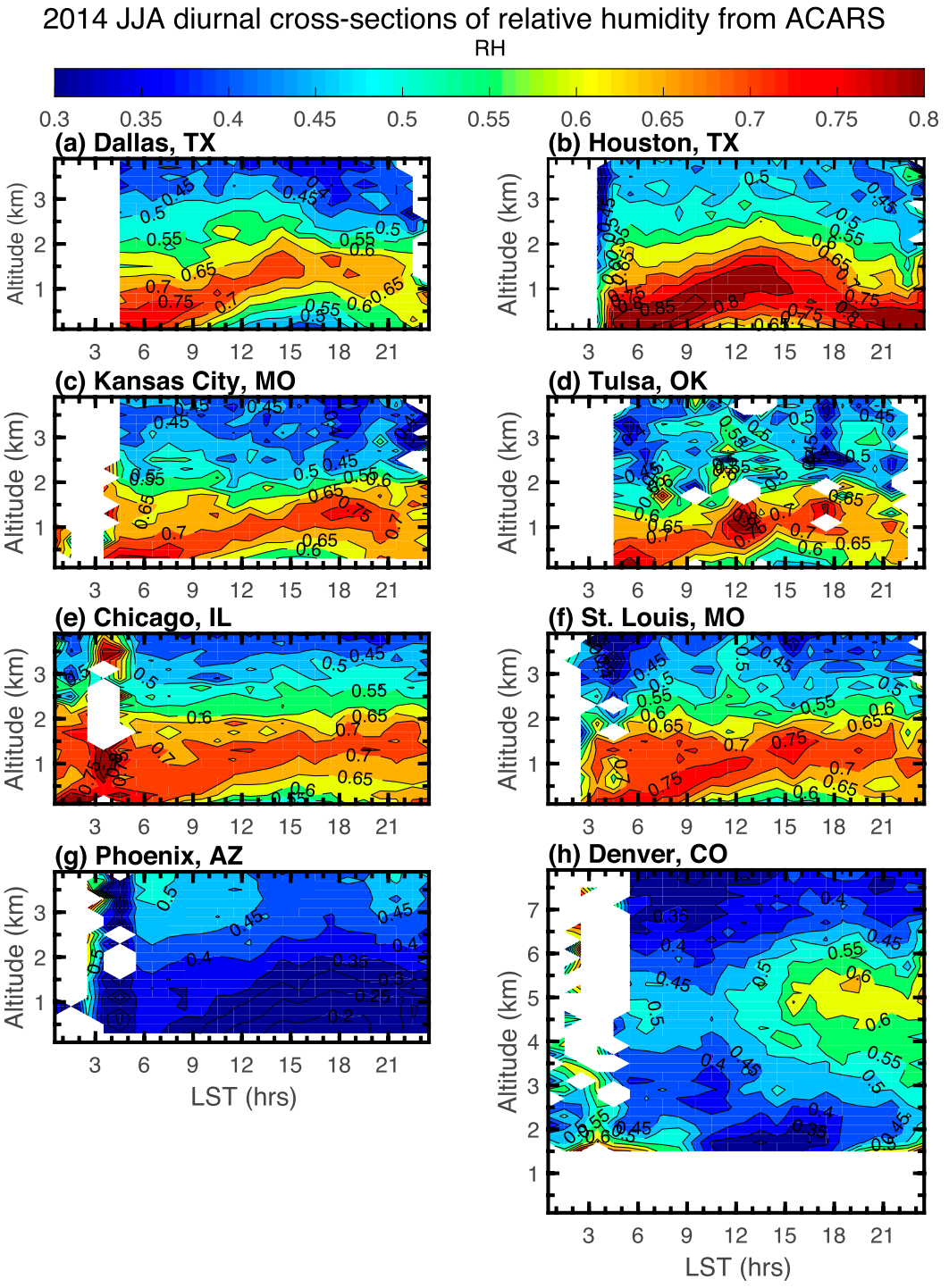

FIG. 10. JJA 2014 cross sections of relative humidity at (a) Dallas, (b) Houston, (c) Kansas City, (d) Tulsa, (e) Chicago, (f) St. Louis, (g) Phoenix, and (h) Denver. In 2014, none of the six midwestern locations exhibit nocturnal relative humidity maxima above the boundary layer.

For comparison, Fig. 10 shows 2014 JJA diurnal vertical cross sections of relative humidity at the same locations. The nocturnal 2–3-km relative humidity maximum is not present at any of the six midwestern locations or Phoenix. Changes in relative humidity at the midwestern sites therefore appear to be coherent from year to year.

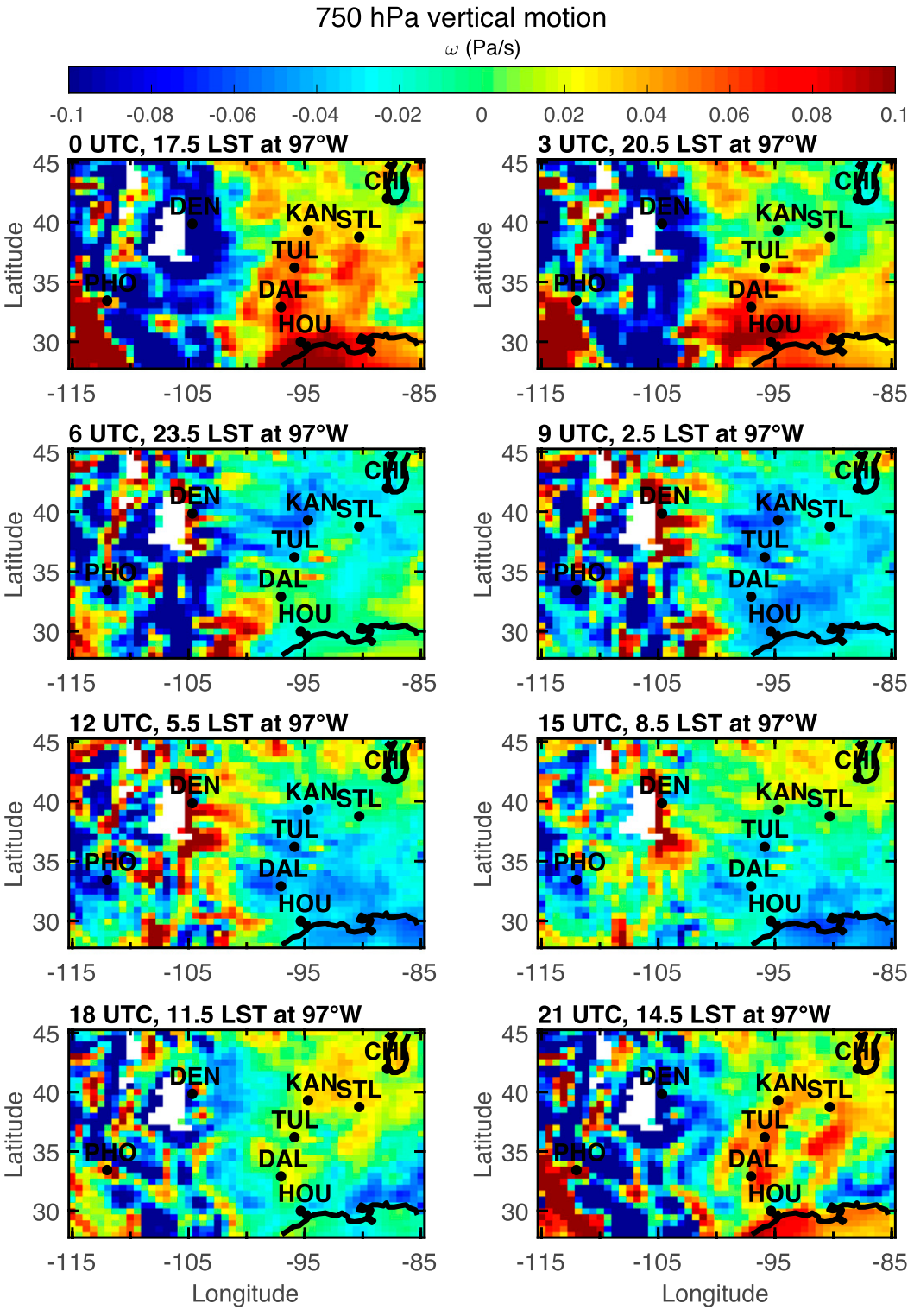

FIG. 11. Spatial and diurnal variation of JJA 750-hPa vertical motion (Pa s^{-1}) from MERRA-2. Data from JJA of 2005–14 are used in order to be consistent with the ACARS time period. Note the daytime downward motion and nocturnal upward motion at each of the six midwestern sites.

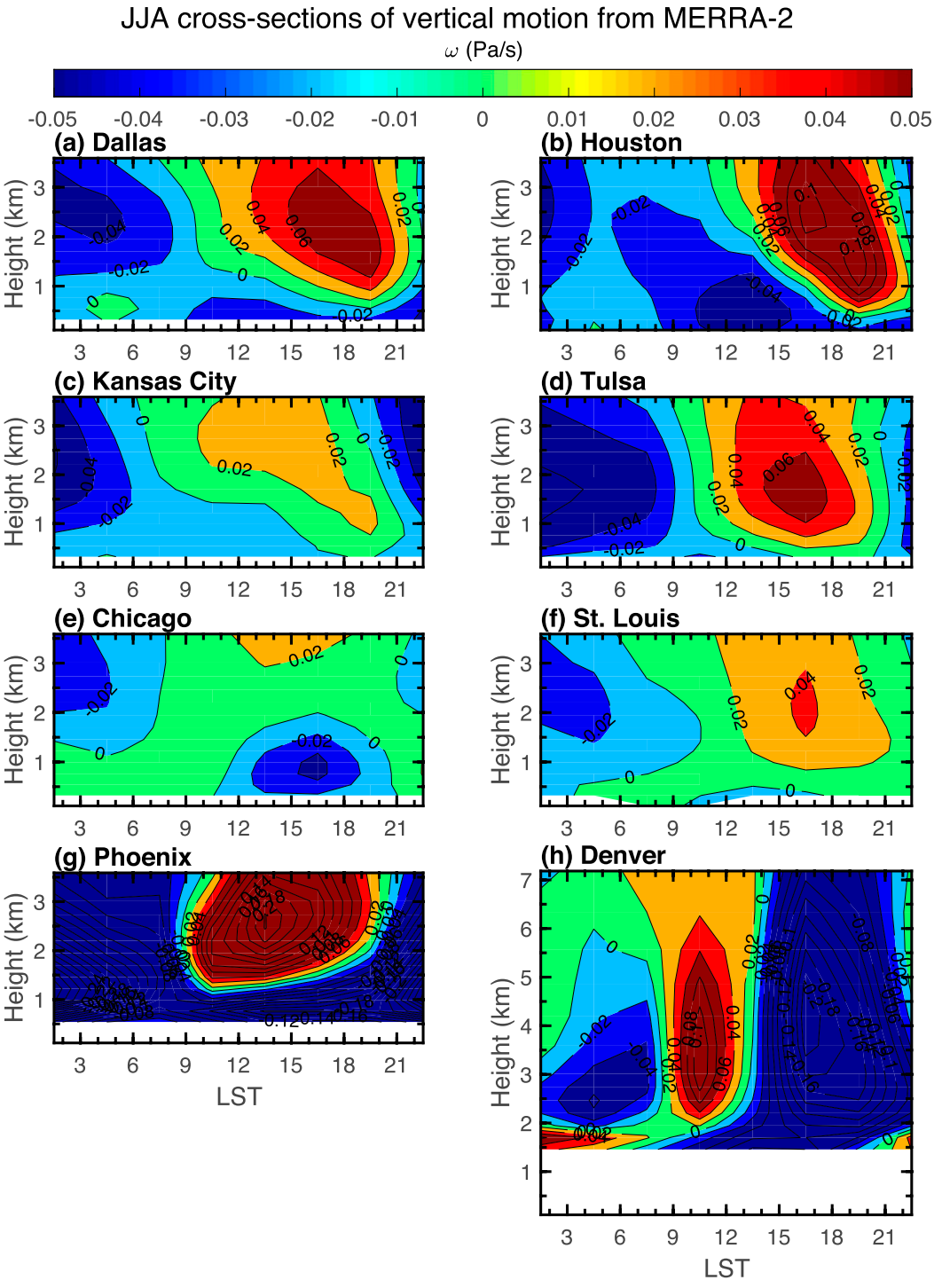

FIG. 12. JJA cross sections of vertical motion (Pa s^{-1}) at (a) Dallas, (b) Houston, (c) Kansas City, (d) Tulsa, (e) Chicago, (f) St. Louis, (g) Phoenix, and (h) Denver from MERRA-2. Data are averaged over JJA of 2005–14. At the six midwestern sites, there is upward motion between 2 and 3 km overnight.

Although not shown, we examined Tropical Rainfall Measuring Mission (TRMM; Huffman et al. 2007) rainfall measurements over the Midwest during each summer from 2005 to 2014. There were no consistent differences in diurnal rainfall variation during years in which the nocturnal relative humidity maxima were stronger.

5. MERRA-2 vertical motion and relative humidity

The vertical motion associated with the mountain–plains solenoid is likely to affect the diurnal variation of relative humidity in the lower troposphere. We use MERRA-2 reanalysis data to show the spatial and diurnal variation of 750-hPa vertical motion over the continental United States. Figure 11 shows the spatial variation of 750-hPa vertical motion every 3 h, within the 28°–45°N, 115°–75°W domain, using JJA data from 2005 to 2014. Coastlines are outlined in black. The eight airport locations are labeled in black.

The times (in LST) in Fig. 11 are defined with respect to 97°W. At 1430, 1730, and 2030 LST, there is upward motion over the mountains (blue) and widespread downward motion over the plains (red). The downward motion over the plains is strongest at 1730 and 2030 LST. Overnight, at 0230, 0530, and 0830 LST, there is downward motion over the mountains and widespread upward motion over the plains. Upward motion over the plains is strongest at 0230 LST.

White spaces in Fig. 11 indicate that there are either no data in a given grid box or that the data have been screened out. Over high orography, surface pressure is often lower than 750 hPa and there are no measurements. If within a given latitude–longitude grid box, at least 10% of the data over the 10 summers is undefined, then the box is shaded white.

Figure 12 shows diurnal cross sections of vertical motion at each of the eight airport locations during JJA of 2005–14, using data from the grid box nearest each airport. The six midwestern airport locations have broadly similar diurnal patterns. During the afternoon and evening, there is downward motion that is strongest near 2 km. Overnight, there is upward motion between 2 and 3 km. This upward motion is coincident with the height and timing of the relative humidity maxima observed at these six airports. At Phoenix, there is very strong downward motion between 1 and 4 km from roughly 0900 to 2100 LST, and strong upward motion at night. At Denver, there is very strong upward motion at all height levels shown from 1400 to 2200 LST, weaker upward motion between 2 and 4 km overnight, and downward motion between 2 and 5 km from 0900 to 1200 LST.

Figure 13 shows the diurnal cycle of 750-hPa vertical motion at Dallas during each season of 2011. The diurnal variation of vertical motion is weakest in winter (November–February), increases during spring (March–April), is strongest during summer (May–August), and weakens in the fall (September–October).

Figure 14 shows diurnal cross sections of MERRA-2 relative humidity during JJA 2011 at each of the eight airport locations. The overall diurnal variation of

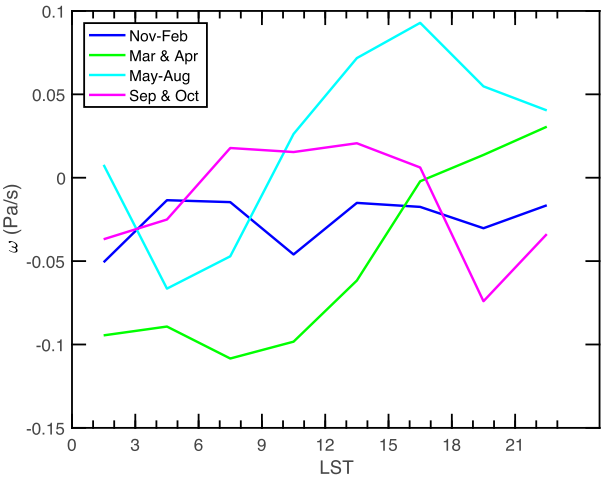

FIG. 13. Seasonal variation in 750-hPa vertical motion (Pa s^{-1}) at Dallas during 2011. The largest diurnal variation in vertical motion occurs during the summer months (May–August).

MERRA-2 relative humidity in the boundary layer is similar to that from ACARS (Fig. 9). However, the very distinct 2.5-km nocturnal relative humidity maxima observed during 2011 are either not present, or, in the case of Dallas and Houston, much weaker than observed. At Denver, the observed relative humidity maximum below 3 km between 0300 and 0900 LST shown in Fig. 9 is not captured by the reanalysis.

We investigate to what extent the observed diurnal variation in relative humidity between 2 and 3 km at the midwestern airport locations can be attributed to the diurnal variation in the vertical wind of the MERRA-2 analysis. At a given level, we assume that the diurnal time variation in q and temperature T is given simply by

$$\frac{\partial q}{\partial t} = -\omega \frac{\partial q}{\partial p}, \tag{1}$$

$$\frac{\partial T}{\partial t} = \omega \left(\frac{\Gamma_d - \Gamma}{\rho g} \right), \tag{2}$$

where Γ_d is the dry adiabatic lapse rate, Γ is the environmental lapse rate, ρ is the air density, g is the acceleration caused by gravity, t is time, and p is pressure. These equations assume that horizontal advection of q and T can be neglected, that the flow is adiabatic, that there are no sources or sinks of q, and that the flow is laminar. We also assume that it is appropriate to use the 2005–14 JJA mean of each variable at each diurnal time. In this case, at each airport, $\partial q/\partial t$ and $\partial T/\partial t$ can be calculated as a function of time and height using the appropriate MERRA-2 values of $\partial q/\partial p$, ω, Γ, and ρ. Using the values of q and T at the first diurnal time step, the diurnal variation of q and T can then be calculated.

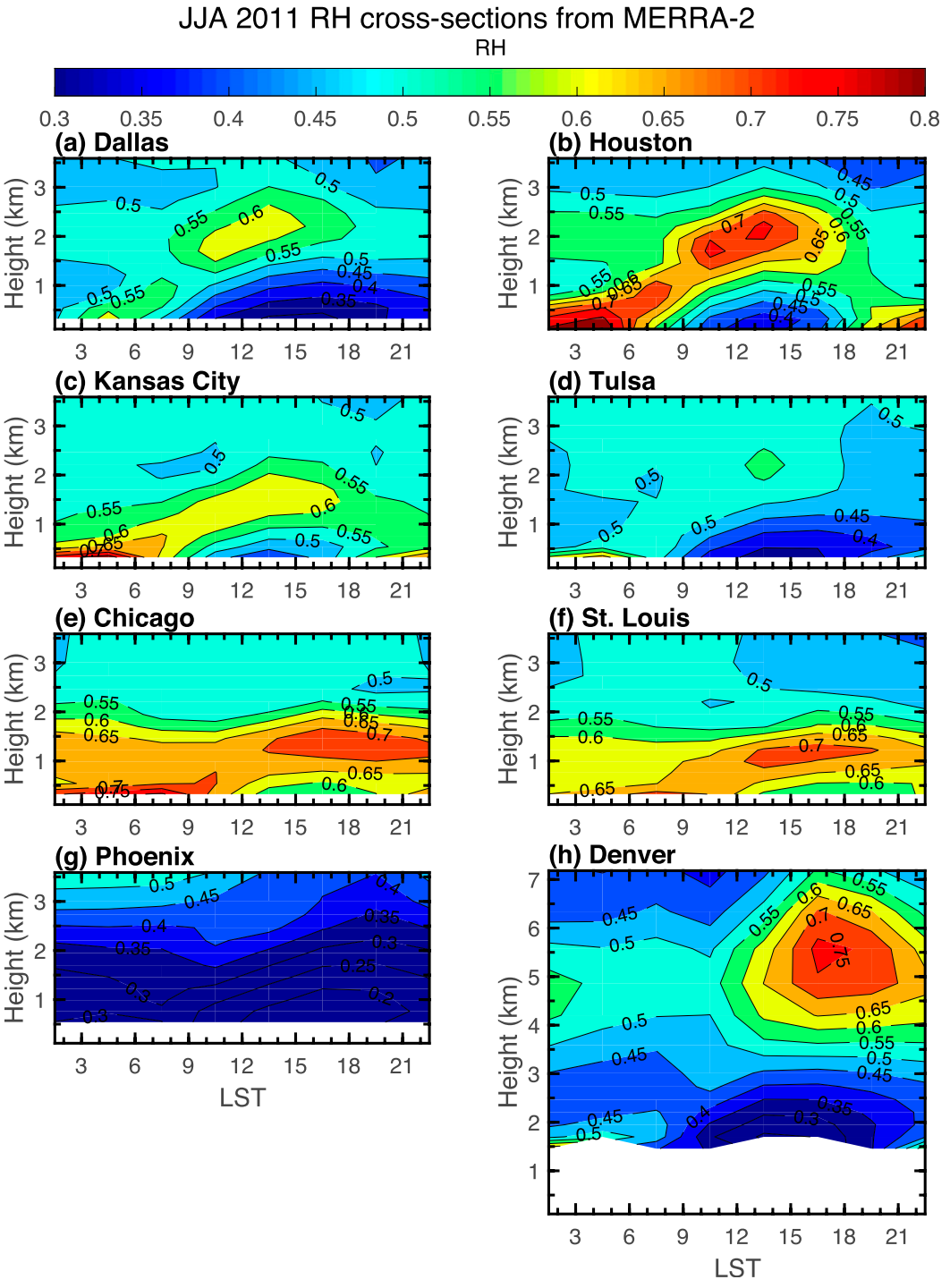

FIG. 14. JJA cross sections of MERRA-2 relative humidity at (a) Dallas, (b) Houston, (c) Kansas City, (d) Tulsa, (e) Chicago, (f) St. Louis, (g) Phoenix, and (h) Denver during 2011. The very strong 2.5-km nocturnal relative humidity maxima observed at the Midwest airports in 2011 is underrepresented in the MERRA-2 analysis.

Figure 15a shows the resulting diurnal variation in the relative humidity anomaly at Dallas, obtained by subtracting the 24-h mean at each height. For comparison, Fig. 15b shows the relative humidity anomalies from the ACARS observations. The diurnal amplitude of the relative humidity anomaly between 2 and 3 km simulated by the MERRA-2 vertical motion is roughly equal to that obtained from the ACARS dataset. However,

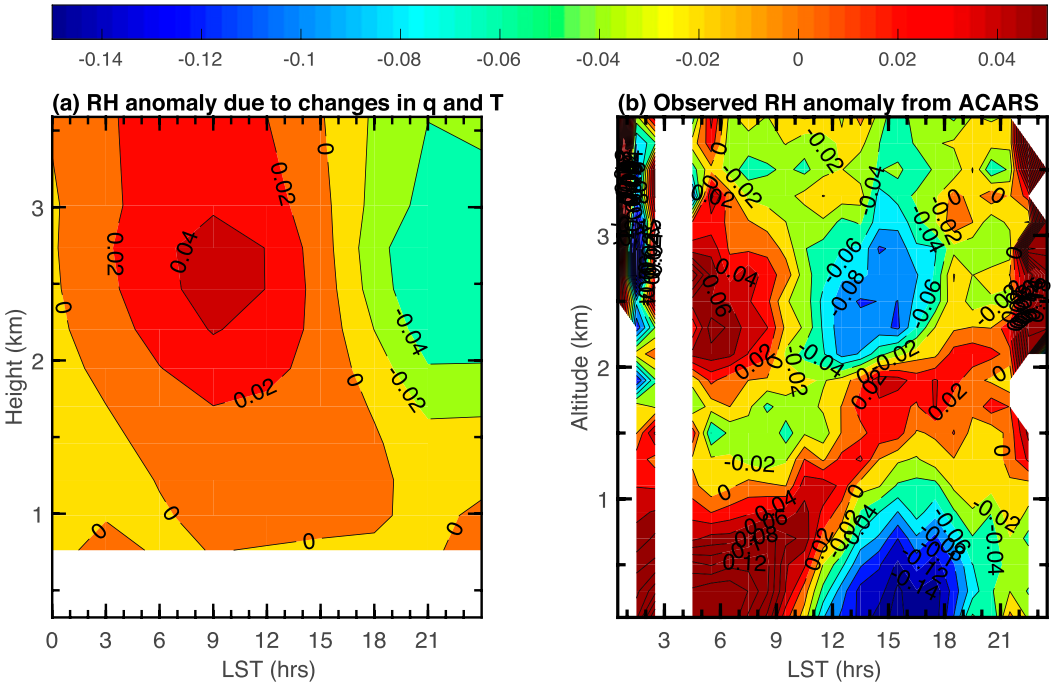

FIG. 15. JJA diurnal cross sections of (a) MERRA-2 relative humidity anomaly at Dallas, associated with diurnal changes in q and T generated by vertical motion, and (b) observed relative humidity anomaly from ACARS.

the simulated relative humidity anomaly lags the observed anomaly by roughly 3 h.

6. Nocturnal LLJ

The nocturnal LLJ is an important source of moisture for nocturnal convection over the Midwest (Stull 1988; Higgins et al. 1997; Berg et al. 2015). The LLJ is also associated with a strong diurnal variation in ageostrophic wind, which would be associated with a diurnal variation in vertical motion. The vertical circulations associated with the LLJ are likely to be coupled with the lower-tropospheric mountain–plains solenoid, and could also be at least partially responsible for the observed nocturnal relative humidity anomalies near 2.5 km.

Figure 16 shows a comparison of ACARS and MERRA-2 diurnal cycles of wind speed (Figs. 16a,b), zonal wind u (Figs. 16c,d), and meridional wind v (Figs. 16e,f) at Dallas. Winds are averaged over JJA 2005–14. In the ACARS observations, the nocturnal LLJ first appears near 2000 LST between 0.5 and 1.5 km and persists until 0800 LST (Fig. 16a). The LLJ is mainly southerly with a weak zonal component that switches from easterly to westerly near midnight. The LLJ is quite well represented by the MERRA-2 reanalysis. For example, the analysis captures the zonal wind direction change near midnight, from easterly to westerly.

In the boundary layer during the day, there is an approximate three-way balance between the pressure gradient force, Coriolis force, and friction (Holton 2004). At sunset, the daytime convective boundary layer collapses, and frictional deceleration associated with turbulent momentum transport becomes restricted to a shallow surface layer. Above this layer, there is an imbalance between the pressure gradient force and the Coriolis force. As a result, winds above the nocturnal boundary layer accelerate and become supergeostrophic (Blackadar 1957). The wind vector then rotates about the geostrophic wind vector in an inertial oscillation. Figure 17 shows a comparison of ACARS and MERRA-2 wind hodographs at Dallas during JJA 2005–14. Unlike traditional hodographs, the points represent different times of day (LST). The colors represent different heights and are labeled in the plot legends.

Both the ACARS and MERRA-2 hodographs have a circular shape. The sizes of the circles roughly represent the magnitude of the diurnal variation of friction at each height. The largest diurnal variation in friction occurs between 500 and 900 m. Figure 16a shows that the LLJ maximum lays between these heights. Below and above this height interval, the circles are much smaller. Near 2 km (above the daytime boundary layer), the diurnal variation of friction appears to approach zero.

7. Conclusions

We have used measurements from commercial aircraft to show that, during the summer, there are

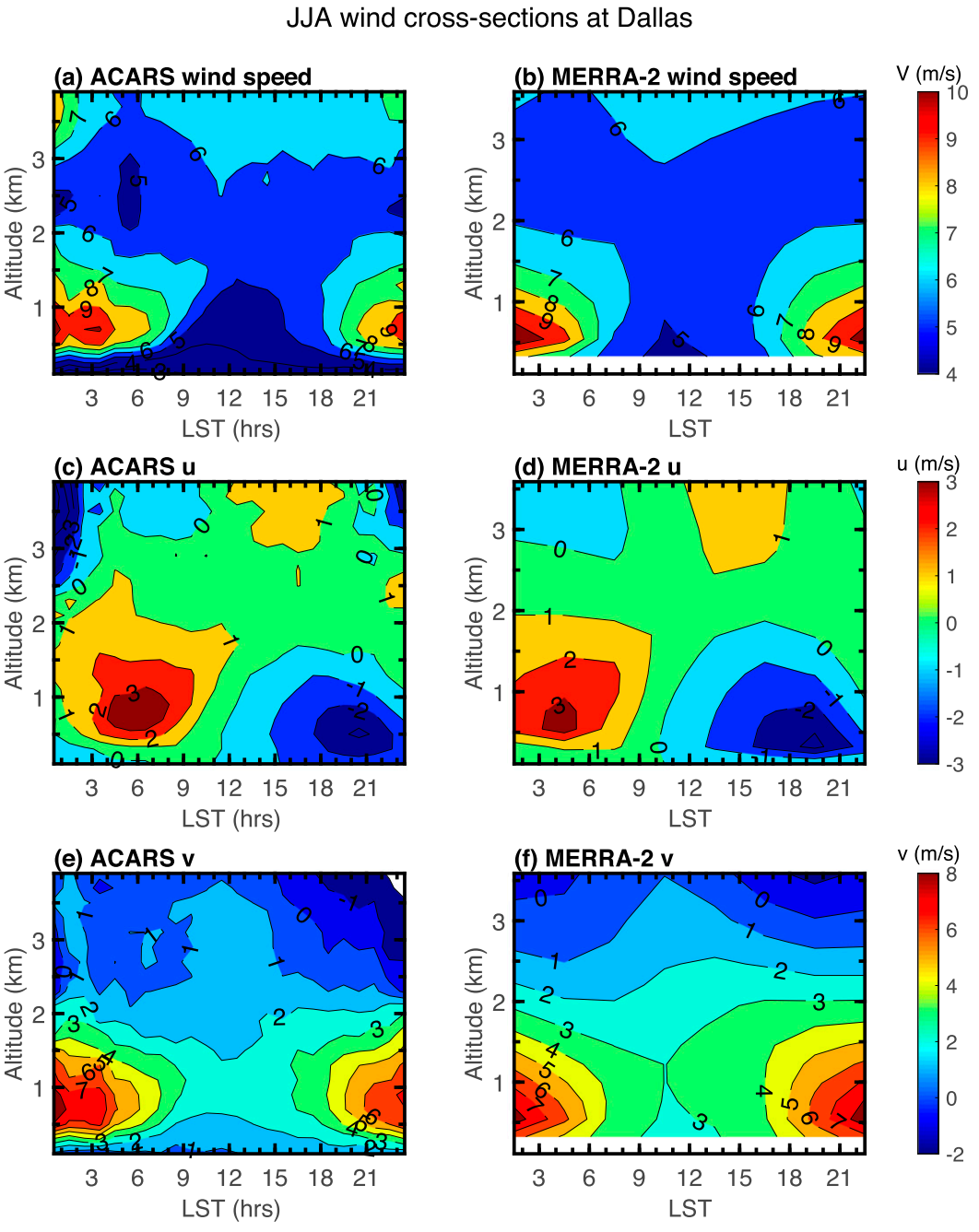

FIG. 16. JJA mean diurnal cross sections of (a),(b) wind speed; (c),(d) u; and (e),(f) v in the Dallas area from ACARS and MERRA-2 ($m\,s^{-1}$). Data from 2005 to 2014 are used. The nocturnal LLJ maximum spans between 500 and 900 m. The zonal direction of the LLJ switches from easterly to westerly near midnight.

overnight maxima in relative humidity between 2 and 3 km at six airports in the U.S. Midwest. These relative humidity maxima are associated with negative anomalies in temperature and positive anomalies in specific humidity, as would be expected if they were generated by upward motion. We used MERRA-2 reanalysis data to show that, at each of these six airports, there is a diurnal variation in vertical motion in the lower troposphere with downward motion during the day and upward motion at night. The nocturnal relative humidity maxima, therefore, provide the strongest direct observational evidence to date of the existence of the mountain–plains solenoid, and offer a diagnostic for testing the strength of

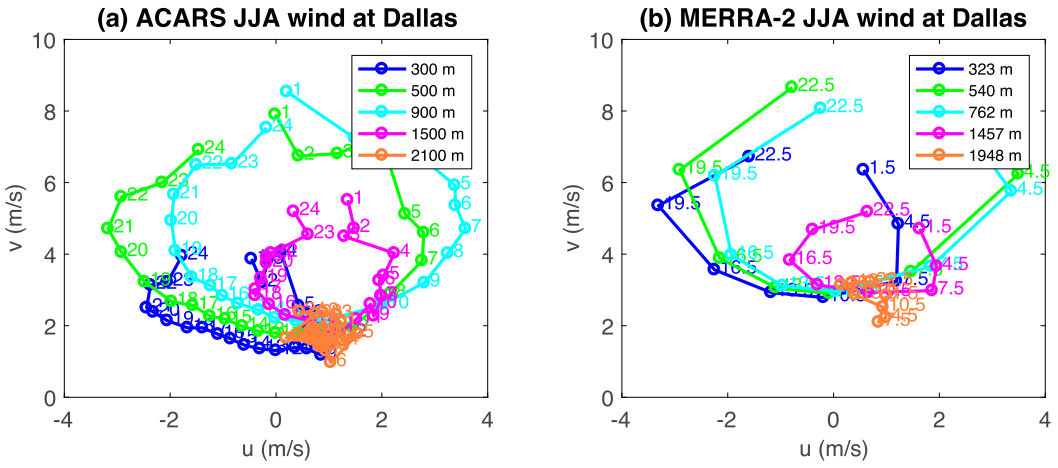

FIG. 17. JJA hodographs (m s^{-1}) at Dallas from (a) ACARS and (b) MERRA-2. Here, points represent different local times and the colors represent different heights. Note the circular shape of each hodograph from both datasets. The larger the circle, the greater the diurnal variation of friction.

this diurnal circulation in climate models and reanalysis datasets.

The magnitude of the nocturnal relative humidity maxima appear to be underrepresented in the MERRA-2 reanalysis. However, the diurnal variation in MERRA-2 vertical motion at Dallas appears to be sufficiently strong that it would be able to generate a diurnal variation in relative humidity above the boundary layer of roughly the magnitude observed.

There is significant interannual variability in the magnitude of the summer nocturnal relative humidity maxima. This variability is coherent from year to year across each of the six Midwestern airports. In 2011, for example, this feature was extremely strong, while in other years, such as 2014, it was almost nonexistent. This is consistent with modeling studies that show that the mountain–plains solenoid is a delicate circulation whose strength can be modulated by the larger-scale circulation or by surface properties such as soil moisture (Wolyn and McKee 1994). Though not shown, we examined rain records for the years in which the maxima were weaker and stronger. We did not see any consistent changes in the diurnal rainfall variation, and have not been able to identify the origin of the interannual variability. Progress in identifying the origin of the dynamical variability in the strength of the solenoidal circulation will likely require relative humidity measurements in the lower troposphere over the U.S. Midwest that are capable of resolving variability on both diurnal and synoptic time scales.

Although the nocturnal relative humidity maxima are strongest during the summer months, they are present to some degree in the spring and fall. The strength of the mountain–plains solenoidal circulation should roughly scale with the strength of solar heating over the mountains. The seasonal variation of the relative humidity maxima is, therefore, also consistent with forcing by the mountain–plains solenoid.

The nocturnal LLJ is an important source of moisture to the U.S. Midwest (Berg et al. 2015; Pitchford and London 1962; Higgins et al. 1997), and is associated with strong horizontal ageostrophic and vertical motions in the boundary layer. As such, it can also be expected to modulate the diurnal variation of relative humidity in the boundary layer, and to some extent, the diurnal variation of relative humidity in the lower free troposphere as well. However, because the diurnal variability in horizontal wind associated with the LLJ is restricted to below 2 km, it is not likely to be the main source of diurnal variability in relative humidity between 2 and 3 km.

We also examined the diurnal variation in lower-tropospheric relative humidity at Phoenix and Denver. These two locations are much closer to strong sources of orographic solar heating. As a result, the diurnal variation in lower-tropospheric vertical motion at these two locations can be expected to be much stronger than at the six midwestern locations. At Phoenix, there is a strong positive anomaly in relative humidity at night between 2 and 3 km. At Denver, there is a strong positive relative humidity anomaly starting in the afternoon. These diurnal variations in relative humidity are consistent with the strong diurnal variation in vertical motion at these two locations in the MERRA-2 reanalysis.

Acknowledgments. This study was supported by grants from the Natural Sciences and Engineering Research Council of Canada (NSERC) and the Marine Environmental Observation Prediction and Response Network (MEOPAR). We thank Glen Lesins, Jeff Geddes, and Brian Boys for their useful suggestions. We would also like

to thank two anonymous referees for their very careful and helpful reviews of the manuscript.

REFERENCES

Bao, X., and F. Zhang, 2013: Impacts of the mountain-plains solenoid and cold pool dynamics on the diurnal variation of warm-season precipitation over northern China. *Atmos. Chem. Phys.*, **13**, 6965–6982, https://doi.org/10.5194/acp-13-6965-2013.

Benjamin, S., B. Schwartz, and R. Cole, 1999: Accuracy of ACARS wind and temperature observations determined by collocation. *Wea. Forecasting*, **14**, 1032–1038, https://doi.org/10.1175/1520-0434(1999)014<1032:AOAWAT>2.0.CO;2.

Berg, L., L. Riihimaki, Y. Qian, H. Yan, and M. Huang, 2015: The low-level jet over the Southern Great Plains determined from observations and reanalyses and its impact on moisture transport. *J. Climate*, **28**, 6682–6706, https://doi.org/10.1175/JCLI-D-14-00719.1.

Blackadar, A., 1957: Boundary layer wind maxima and their significance for the growth of nocturnal inversions. *Bull. Amer. Meteor. Soc.*, **38**, 283–290.

Bossert, J., J. Sheaffer, and E. Reiter, 1989: Aspects of regional-scale flows in mountainous terrain. *J. Appl. Meteor.*, **28**, 590–601, https://doi.org/10.1175/1520-0450(1989)028<0590:AORSFI>2.0.CO;2.

Carbone, R., and J. Tuttle, 2008: Rainfall occurrence in the U.S. warm season: The diurnal cycle. *J. Climate*, **21**, 4132–4146, https://doi.org/10.1175/2008JCLI2275.1.

Gelaro, R., and Coauthors, 2017: The Modern-Era Retrospective Analysis for Research and Applications, version 2 (MERRA-2). *J. Climate*, **30**, 5419–5454, https://doi.org/10.1175/JCLI-D-16-0758.1.

GMAO, 2015: MERRA-2 inst3_3d_asm_Np: 3d, 3-hourly, instantaneous, pressure-level assimilation, assimilated meteorological fields, version 5.12.4. Goddard Earth Sciences Data and Information Services Center (GES DISC), accessed 4 April 2017, doi:10.5067/QBZ6MG944HW0.

Higgins, R., Y. Yao, E. Yarosh, J. Janowiak, and K. Mo, 1997: Influence of the Great Plains low-level jet on summertime precipitation and moisture transport over the central United States. *J. Climate*, **10**, 481–507, https://doi.org/10.1175/1520-0442(1997)010<0481:IOTGPL>2.0.CO;2.

Holton, J., 2004: *An Introduction to Dynamic Meteorology*. Academic Press, 535 pp.

Huffman, G., and Coauthors, 2007: The TRMM Multisatellite Precipitation Analysis (TMPA): Quasi-global, multiyear, combined-sensor precipitation estimates at fine scales. *J. Hydrometeor.*, **8**, 38–55, https://doi.org/10.1175/JHM560.1.

Li, Y., and R. Smith, 2010: The detection and significance of diurnal pressure and potential vorticity anomalies east of the Rockies. *J. Atmos. Sci.*, **67**, 2734–2751, https://doi.org/10.1175/2010JAS3423.1.

Mamrosh, R., R. Baker, and T. Jirikowic, 2002: A comparison of ACARS WVSS and NWS radiosonde temperature and moisture data. *Sixth Symp. on Integrated Observing Systems*, Orlando, FL, Amer. Meteor. Soc., 6.1.4, https://ams.confex.com/ams/pdfpapers/30088.pdf.

McCarty, W., L. Coy, R. Gelaro, A. Huang, D. Merkova, E. Smith, M. Sienkiewicz, and K. Wargan, 2016: MERRA-2 input observations: Summary and assessment. NASA Tech. Rep. NASA/TM-2016-104606, Vol. 46, 51 pp., https://gmao.gsfc.nasa.gov/pubs/docs/McCarty885.pdf.

Moninger, W., R. Mamrosh, and P. Pauley, 2003: Automated meteorological reports from commercial aircraft. *Bull. Amer. Meteor. Soc.*, **84**, 203–216, https://doi.org/10.1175/BAMS-84-2-203.

Nicolini, M., and Y. G. Skabar, 2011: Diurnal cycle in convergence patterns in the boundary layer east of the Andes and convection. *Atmos. Res.*, **100**, 377–390, https://doi.org/10.1016/j.atmosres.2010.09.019.

Pitchford, K., and J. London, 1962: The low-level jet as related to nocturnal thunderstorms over Midwest United States. *J. Appl. Meteor.*, **1**, 43–47, https://doi.org/10.1175/1520-0450(1962)001<0043:TLLJAR>2.0.CO;2.

Rabenhorst, S., D. Whiteman, D.-L. Zhang, and B. Demoz, 2014: A case study of Mid-Atlantic nocturnal boundary layer events during WAVES 2006. *J. Appl. Meteor. Climatol.*, **53**, 2627–2648, https://doi.org/10.1175/JAMC-D-13-0350.1.

Repinaldo, H. F. B., M. Nicolini, and Y. G. Skabar, 2015: Characterizing the diurnal cycle of low-level circulation and convergence using CFSR data in southeastern South America. *J. Appl. Meteor. Climatol.*, **54**, 671–690, https://doi.org/10.1175/JAMC-D-14-0114.1.

Schwartz, B., and S. Benjamin, 1995: A comparison of temperature and wind measurements from ACARS-equipped aircraft and rawinsondes. *Wea. Forecasting*, **10**, 528–544, https://doi.org/10.1175/1520-0434(1995)010<0528:ACOTAW>2.0.CO;2.

Smith, A., N. Lott, T. Houston, K. Shein, J. Crouch, and J. Enloe, 2017: U.S. billion-dollar weather and climate disasters 1980–2017. NOAA National Centers for Environmental Information (NCEI), 13 pp., https://www.ncdc.noaa.gov/billions/events.pdf.

Stull, R. B., 1988: *An Introduction to Boundary Layer Meteorology*. Kluwer Academic, 666 pp.

Sullivan, J., and Coauthors, 2016: Quantifying the contribution of thermally driven recirculation to a high-ozone event along the Colorado Front Range using lidar. *J. Geophys. Res. Atmos.*, **121**, 10 377–10 390, https://doi.org/10.1002/2016JD025229.

Sun, J., and F. Zhang, 2012: Impacts of mountain–plains solenoid on diurnal variations of rainfalls along the mei-yu front over the east China plains. *Mon. Wea. Rev.*, **140**, 379–397, https://doi.org/10.1175/MWR-D-11-00041.1.

Trier, S., C. Davis, and D. Ahijevych, 2010: Environmental controls on the simulated diurnal cycle of warm-season precipitation in the continental United States. *J. Atmos. Sci.*, **67**, 1066–1090, https://doi.org/10.1175/2009JAS3247.1.

Tripoli, G., and W. Cotton, 1989: Numerical study of an observed orogenic mesoscale convective system. Part 1: Simulated genesis and comparison with observations. *Mon. Wea. Rev.*, **117**, 273–304, https://doi.org/10.1175/1520-0493(1989)117<0273:NSOAOO>2.0.CO;2.

Tuttle, J., and C. Davis, 2013: Modulation of the diurnal cycle of warm-season precipitation by short-wave troughs. *J. Atmos. Sci.*, **70**, 1710–1726, https://doi.org/10.1175/JAS-D-12-0181.1.

Whiteman, C., X. Bian, and S. Zhong, 1997: Low-level jet climatology from enhanced rawinsonde observations at a site in the Southern Great Plains. *J. Appl. Meteor.*, **36**, 1363–1376, https://doi.org/10.1175/1520-0450(1997)036<1363:LLJCFE>2.0.CO;2.

Wolyn, P., and T. McKee, 1994: The mountain–plains circulation east of a 2-km-high north–south barrier. *Mon. Wea. Rev.*, **122**, 1490–1508, https://doi.org/10.1175/1520-0493(1994)122<1490:TMPCEO>2.0.CO;2.

Zhang, Y., F. Zhang, and J. Sun, 2014: Comparison of the diurnal variations of warm-season precipitation for East Asia vs. North America downstream of the Tibetan Plateau vs. the Rocky Mountains. *Atmos. Chem. Phys.*, **14**, 10 741–10 759, https://doi.org/10.5194/acp-14-10741-2014.